

Vertical natural convection: application of the unifying theory of thermal convection

Chong Shen Ng^{1†}, Andrew Ooi¹, Detlef Lohse² and Daniel Chung¹

¹Department of Mechanical Engineering, The University of Melbourne, Victoria 3010, Australia

²Physics of Fluids Group, Faculty of Science and Technology, J. M. Burgers Center for Fluid Dynamics and MESA+ Institute, University of Twente, 7500 AE Enschede, The Netherlands

(Received ?; revised ?; accepted ?. - To be entered by editorial office)

Results from direct numerical simulations of vertical natural convection at Rayleigh numbers 1.0×10^5 – 1.0×10^9 and Prandtl number 0.709 support a generalised applicability of the Grossmann–Lohse (GL) theory, which was originally developed for horizontal natural (Rayleigh–Bénard) convection. In accordance with the GL theory, it is shown that the boundary-layer thicknesses of the velocity and temperature fields in vertical natural convection obey laminar-like Prandtl–Blasius–Pohlhausen scaling. Specifically, the normalised mean boundary-layer thicknesses scale with the $-1/2$ -power of a wind-based Reynolds number, where the “wind” of the GL theory is interpreted as the maximum mean velocity. Away from the walls, the dissipation of the turbulent fluctuations, which can be interpreted as the “bulk” or “background” dissipation of the GL theory, is found to obey the Kolmogorov–Obukhov–Corrsin scaling for fully developed turbulence. In contrast to Rayleigh–Bénard convection, the direction of gravity in vertical natural convection is parallel to the mean flow. The orientation of this flow presents an added challenge because there no longer exists an exact relation that links the normalised global dissipations to the Nusselt, Rayleigh and Prandtl numbers. Nevertheless, we show that the unclosed term, namely the global-averaged buoyancy flux that produces the kinetic energy, also exhibits both laminar and turbulent scaling behaviours, consistent with the GL theory. The present results suggest that, similar to Rayleigh–Bénard convection, a pure power-law relationship between the Nusselt, Rayleigh and Prandtl numbers is not the best description for vertical natural convection and existing empirical relationships should be recalibrated to better reflect the underlying physics.

1. Introduction

In the study of pure buoyancy-driven flow (natural convection) between two differentially heated vertical surfaces (figure 1 *a*), there has been an ongoing interest for establishing a general relationship between the heat transfer and the temperature difference for an arbitrary fluid. The heating and cooling that occurs in this vertical setup is a fundamental problem that is often found in applications such as building ventilation, computer systems and power plants. The relevant parameters are the Nusselt number Nu , that is, the dimensionless heat transfer rate; the Rayleigh number Ra , that is, the dimensionless temperature difference; and the Prandtl number Pr , that is, the ratio of fluid viscosity to the thermal diffusivity. Past studies have shown a preference for the power-law form, $Nu \sim Ra^p$ (at fixed Pr), but the exponent p has been reported to range anywhere between $1/3$ and $1/4$ (Batchelor 1954; Elder 1965; Churchill & Chu 1975; George & Capp

[†] Email address for correspondence: chongn@unimelb.edu.au

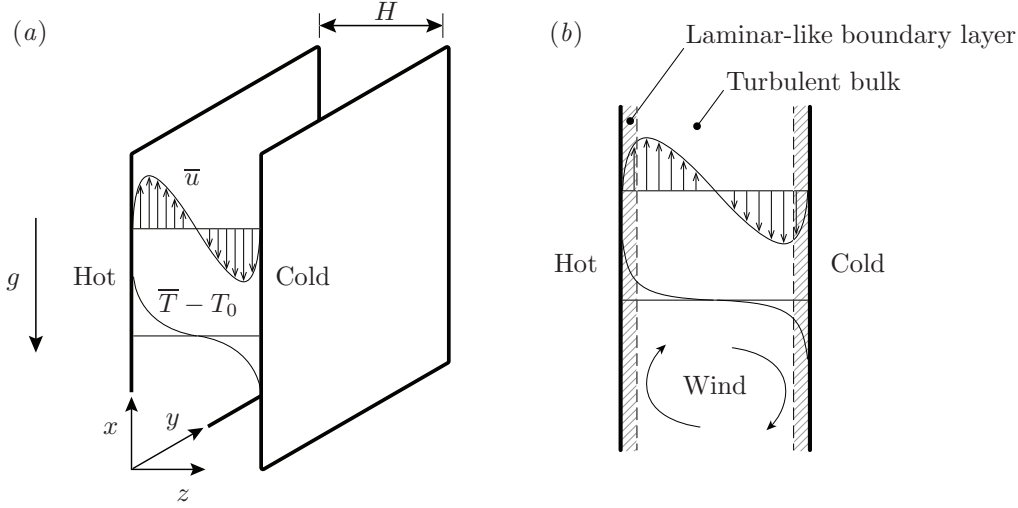


Figure 1: (a) Setup of vertical natural convection and (b) illustration of the laminar-like (boundary-layer) and turbulent (bulk) regions of the Grossmann-Lohse theory.

1979; Tsuji & Nagano 1988; Versteegh & Nieuwstadt 1999; Kiš & Herwig 2012; Ng *et al.* 2013). A careful examination of recent direct numerical simulation (DNS) data (figure 2) demonstrates this point: there is no range in which Nu/Ra^p is constant and the effective power-law exponents depend on Ra and is less than $1/3$ but greater than $1/4$. Thus, a pure power law may not be the best description of the heat-transfer relationship. One approach is a power-law fit of arbitrary exponent to the existing data (e.g. $p \approx 0.31$ in figure 2a), but this ignores the underlying flow physics and is therefore risky when applied outside the range of calibration.

A similar scaling behaviour has also been reported in horizontal, i.e. Rayleigh-Bénard (RB), natural convection (e.g. Stevens *et al.* 2011). In RB convection, the unifying theory of Grossmann & Lohse (2000, 2001, 2002, 2004) (hereafter GL theory) offered a resolution to the previously experimentally found (Castaing *et al.* 1989; Chavanne *et al.* 1997, 2001) but unexplained $Nu \sim Ra^{0.289}$ behaviour (for unity Pr) by showing that the physics-unaware 0.289-power can be understood as a combination of a $1/4$ - and a $1/3$ -power-law scaling. The latter two exponents can be readily linked to distinct flow regimes. The GL theory works because it accounts for the possibility that, at moderate Rayleigh numbers and away from the walls, the buoyancy-driven turbulent “wind” is not sufficiently strong to drive a turbulent boundary layer in the classical sense of Prandtl and von Kármán. The theory has since been further articulated and vetted by both experiments and simulations across a large range of Ra and Pr (e.g. Ahlers *et al.* 2009; Stevens *et al.* 2013). The theory has also been extended to other related flows, including rotating RB convection (Stevens *et al.* 2010a) and Taylor-Couette flow (Eckhardt *et al.* 2007). The success of the GL theory and the similarities between RB and vertical natural convection motivates the present study.

In the following, we investigate a generalised application of the ideas of the GL theory to vertical natural convection through a close examination of the present DNS data (described in § 2) for $Ra = 1.0 \times 10^5 - 1.0 \times 10^9$ and $Pr = 0.709$. Many elements of the GL theory apply to vertical natural convection. Since the velocity is non-zero in the mean, the wind of the GL theory is readily identified and Prandtl-Blasius-Pohlhausen scaling of the boundary layers is easily verified (§ 3.1). The “bulk” or “background” flow regime (refer

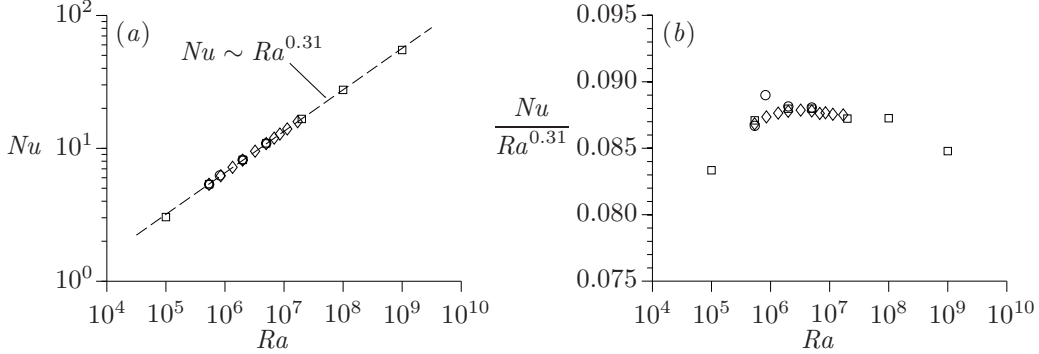


Figure 2: Trend of Nu versus Ra from recent DNS data for air ($Pr = 0.709$): \square , present simulations; \circ , Versteegh & Nieuwstadt (1999); \diamond , Kiš & Herwig (2012). (a) $Nu \sim Ra^p$, where $p \approx 0.31$ from a least-squares fit to a power law; (b) compensated form, Nu/Ra^p versus Ra . The trend exhibits neither a $1/4$ - nor a $1/3$ -power scaling.

to figure 1 b) described by Kolmogorov–Obukhov–Corrsin scaling is also exhibited by the dissipation of turbulent fluctuations (§ 3.2). Apart from the obvious similarities, vertical natural convection is different to RB convection in one important respect: the horizontal direction of heat transfer in vertical natural convection is orthogonal to the vertical direction of the buoyancy flux, which is the source of turbulent kinetic energy. The heat flux and the buoyancy flux coincide in RB convection. Consequently, an exact relationship linking the global dissipation rate with Nu , Ra and Pr no longer exists (§ 3.3). However, it can be shown that the unclosed global-averaged buoyancy flux also exhibits both laminar and turbulent scaling behaviours, consistent with the GL theory. We conclude in § 4 by summarising current progress and speculate on future directions towards establishing closure for a generalised heat-transfer law for vertical natural convection.

2. Flow setup and direct numerical simulations

2.1. Flow setup

We adopt the Boussinesq approximation in which density fluctuations are small relative to the mean. In this incompressible-flow approximation, the density fluctuation, which is linearly related to the temperature fluctuation, is dynamically significant only through the buoyancy force. The temperature difference, $\Delta T = T_h - T_c$, between the hot and cold bounding walls drives the fully developed turbulent natural convection (figure 1 a). The walls are separated by the distance H . The governing continuity, momentum and energy equations are respectively given by,

$$\frac{\partial u_i}{\partial x_i} = 0, \quad (2.1a)$$

$$\frac{\partial u_i}{\partial t} + u_j \frac{\partial u_i}{\partial x_j} = -\frac{1}{\rho_0} \frac{\partial p}{\partial x_i} + \delta_{i1} g \beta (T - T_0) + \nu \frac{\partial^2 u_i}{\partial x_j^2}, \quad (2.1b)$$

$$\frac{\partial T}{\partial t} + u_j \frac{\partial T}{\partial x_j} = \kappa \frac{\partial^2 T}{\partial x_j^2}, \quad (2.1c)$$

where g is the gravitational acceleration, β is the coefficient of thermal expansion, ν is the kinematic viscosity and κ is the thermal diffusivity, all assumed to be independent of temperature. The coordinate system x , y and z (or x_1 , x_2 and x_3) refers to the

Ra	L_x/H	L_y/H	n_x	n_y	n_z	Wall		Centre		$T_{samp}U_{\Delta T}/H$
						$\Delta_{x,y}/\eta$	Δ_z/η	$\Delta_{x,y}/\eta$	Δ_z/η	
1.0×10^5	8	4	384	192	96	1.1	0.1	0.8	0.7	1106
5.4×10^5	8	4	384	192	96	2.0	0.1	1.5	1.2	1010
2.0×10^6	8	4	384	192	96	3.2	0.2	2.3	1.8	862
5.0×10^6	8	4	512	256	96	3.3	0.3	2.4	2.5	788
2.0×10^7	8	4	832	416	192	3.6	0.1	2.4	2.0	802
1.0×10^8	8	4	1536	768	384	3.7	0.1	2.3	1.8	403
1.0×10^9	8	4	3200	1600	768	4.5	0.1	2.6	2.1	7

Table 1: Simulation parameters of the present DNS cases.

streamwise (opposing gravity), spanwise and wall-normal directions. The no-slip and no-penetration boundary conditions are imposed on the velocity at the walls. Periodic boundary conditions are imposed on u_i , p and T in the x - and y -directions. The Rayleigh, Nusselt and Prandtl numbers are respectively defined by,

$$Ra \equiv \frac{g\beta\Delta TH^3}{\nu\kappa}, \quad Nu \equiv \frac{f_w H}{\Delta T\kappa}, \quad Pr \equiv \frac{\nu}{\kappa}, \quad (2.2a,b,c)$$

where $f_w \equiv \kappa|d\bar{T}/dz|_w$, the wall heat flux and $(\cdot)|_w$ denotes the wall value. Presently, $\overline{(\cdot)}$ denotes the spatial xy -plane and $(\cdot)'$ denotes the corresponding fluctuations.

2.2. Direct numerical simulations

In our simulations, the streamwise, spanwise and wall-normal domain sizes, $L_x \times L_y \times L_z$, are $8H \times 4H \times H$ and $Ra = 1.0 \times 10^5$ – 1.0×10^9 (table 1). The fluid is air with $Pr = 0.709$. The present grid spacing is uniform in the x - and y -directions and is stretched by a cosine map in z -direction in order to resolve the steep, near-wall gradients. The resolutions are chosen so that the simulations resolve the Kolmogorov scale, $\eta \equiv [\nu^3/\varepsilon_{u'}]^{1/4}$, where $\varepsilon_{u'}(z) \equiv \nu\overline{(\partial u'_i/\partial x_j)^2}$ is the turbulent dissipation. In the centre of the channel, $\Delta_{x,y,z} < 2.6\eta$, while near the wall, $\Delta_{x,y} < 4.5\eta$ and $\Delta_z < 0.3\eta$. With exception of the highest- Ra case for which computational resources are limited, we report statistics averaged over at least 400 dimensionless turnover times, where a turnover time is defined by the free-fall period, $H/U_{\Delta T}$, where $U_{\Delta T} \equiv (g\beta\Delta TH)^{1/2}$ (cf. Stevens *et al.* 2010b). Higher- Ra cases are initialised using interpolated velocity and temperature fields from lower- Ra cases. Except for the highest- Ra case, the flow is first simulated for more than 70 dimensionless turnover times in order to flush out transients before statistics are sampled. Throughout the sampling duration, Nu remains within 5% of its mean, which is sufficient to ensure a statistically stationary flow (Stevens *et al.* 2010b). The switching between exponential growth in Nu due to the so-called elevator modes, followed by sudden break-down, as observed in so-called homogeneous RB (Calzavarini *et al.* 2005, 2006; Schmidt *et al.* 2012) is not observed in the present flow, as there is no destabilising mean vertical temperature gradient and the flow is bounded by plates. The DNS employs a fully conservative fourth-order staggered finite-difference scheme for the velocity field and the QUICK scheme to advect the temperature field. The equations are marched using a low-storage third-order Runge–Kutta scheme and fractional-step method for enforcing continuity at $\Delta_t = CFL \max_i(\Delta_i/u_i)$, where we set $CFL = 1$ (for details, see Ng *et al.* 2013; Ng 2013). A zero-mass-flux constraint is enforced at every time step to improve

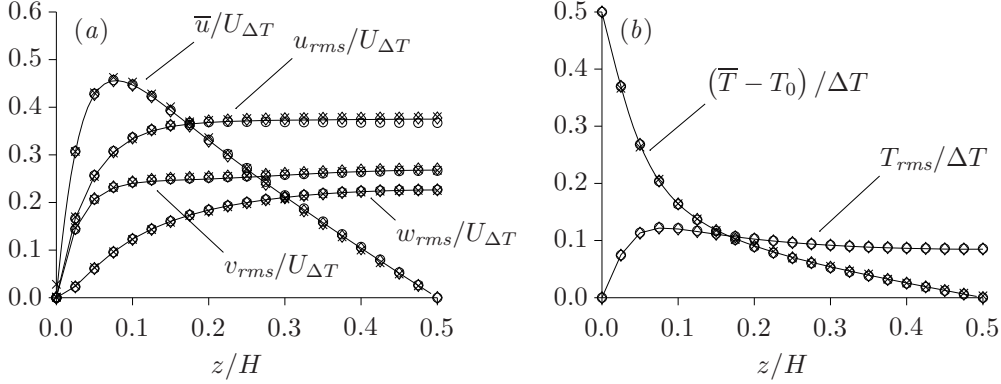


Figure 3: Comparison of mean and second-order turbulent statistics from DNS for (a) velocity and (b) temperature, for $Ra = 5.4 \times 10^5$: —, present simulations; \circ , Versteegh & Nieuwstadt (1999); \times , Pallares *et al.* (2010); \diamond , Kiš & Herwig (2012).

convergence, which is similar to using top and bottom end walls (located far away) in an experiment (e.g. Elder 1965).

Comparisons of the present simulations with other DNS datasets (Versteegh & Nieuwstadt 1999; Pallares *et al.* 2010; Kiš & Herwig 2012) show good agreement for both mean and second-order statistics (figure 3). Throughout this study, statistics are averaged from both halves of the channel, taking the antisymmetry (about the centreline) of the mean profiles into account. The present simulations employ smaller periodic-domain sizes (two-thirds in each periodic direction) than the other DNS studies but are chosen in order to resolve the near-wall region at high Ra . Simulations conducted with the larger periodic-domain sizes showed little difference in the mean and second-order statistics, which are the focus of the present study.

3. Results and discussion

The central idea in the GL theory is to conceptually split the flow into two regions: namely the boundary layer (or plume) and the bulk (or background) regions (Grossmann & Lohse 2000, 2001, 2004). Each of these regions contributes a distinct scaling behaviour to the total kinetic and thermal dissipations, as discussed in the following.

3.1. Scaling of boundary-layer thicknesses

For moderate Ra , the GL theory revealed that the kinetic and thermal boundary-layer thicknesses, δ_u and δ_T , in fact, obey a laminar-like Prandtl–Blasius–Pohlhausen scaling (cf. Landau & Lifshitz 1987):

$$\delta_u/H \sim Re^{-1/2}, \quad \delta_T/H \sim Re^{-1/2} f(Pr), \quad Re \equiv UH/\nu, \quad (3.1a,b,c)$$

where U refers to the wind. To test these predictions, we first need to define U , δ_u and δ_T for vertical natural convection. Unlike RB convection where the (mean) streamwise velocity is zero, the wind is readily identified for the vertical configuration because of the non-zero persistent (mean) streamwise velocity (see figure 1 *a*). Presently, it is defined by $U = \bar{u}_{max}$ (figure 4*a, c*). To define δ_u and δ_T , we adopt definitions based on the gradient of the time- and plane-averaged velocity and temperature profiles at the wall (e.g. Zhou & Xia 2010; Zhou *et al.* 2010; Scheel & Schumacher 2014). The statistical properties of these definitions were also first systematically studied by Sun

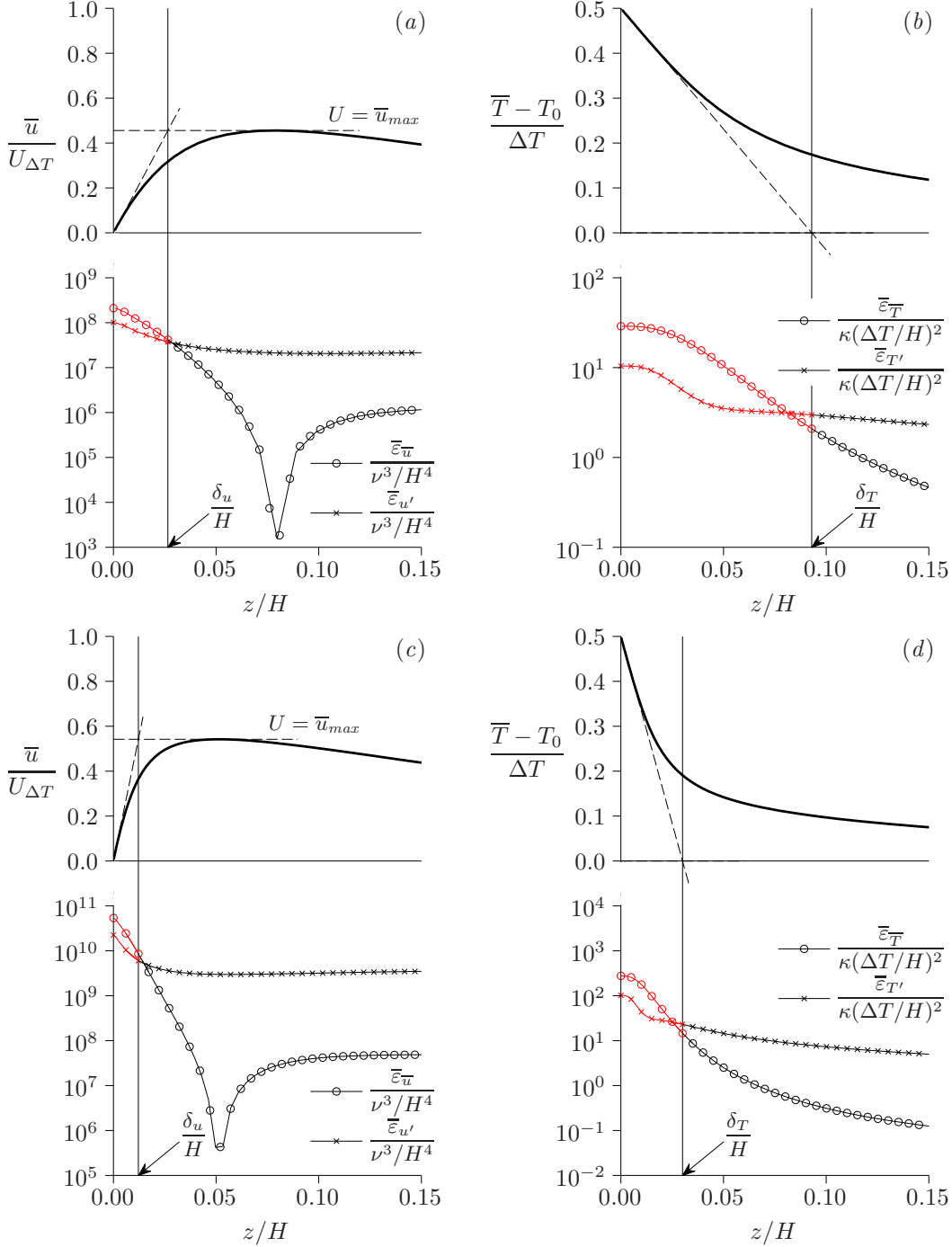


Figure 4: Definitions of the kinetic (δ_u) and thermal (δ_T) boundary-layer thicknesses shown for DNS data at $Ra = 5.4 \times 10^5$ (a, b) and $Ra = 2.0 \times 10^7$ (c, d). The kinetic boundary layer is defined as the wall-distance to the intercept of $\bar{u} = d\bar{u}/dz|_w z$ and $\bar{u} = \bar{u}_{max}$, and the thermal boundary layer is defined as the wall-distance to the intercept of $\bar{T} = T_h + d\bar{T}/dz|_w z$ and $\bar{T} = T_h - \Delta T/2$. These definitions roughly correspond to the crossover points between the mean dissipations and turbulent dissipations, i.e. $\bar{\varepsilon}_{\bar{u}}(\delta_u^d) = \bar{\varepsilon}_{u'}(\delta_u^d)$ and $\bar{\varepsilon}_{\bar{T}}(\delta_T^d) = \bar{\varepsilon}_{T'}(\delta_T^d)$.

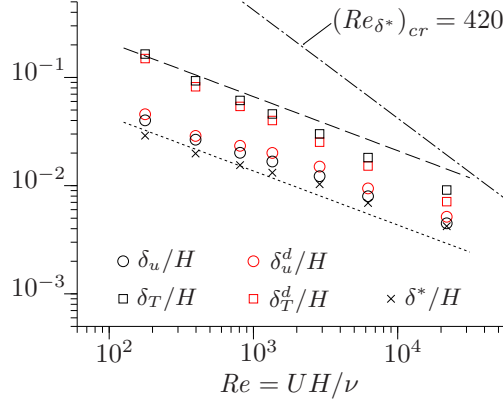


Figure 5: Trends of normalised boundary-layer thicknesses appear to scale with the $-1/2$ -power law of a wind-based Reynolds number. The boundary layer thicknesses are defined as: the distances to the intercepts (figure 4), δ_u/H (\circ) and δ_T/H (\square); the crossovers of dissipation profiles, δ_u^d/H (\odot) and δ_T^d/H (\square^\bullet); and the displacement thickness, δ^*/H (\times). Shown are the Prandtl–Blasius–Pohlhausen $-1/2$ -power scaling predictions for vertical natural convection (3.2) for δ_T (---) and δ_u (.....). As reference, the laminar-to-turbulent transition of the shear boundary layer is expected to occur at $(Re_{\delta^*})_{cr} \approx 420$ (---) (Landau & Lifshitz 1987).

et al. (2008). For the hot wall, the kinetic boundary-layer thickness, δ_u , is defined as the wall-normal distance to the intercept of $\bar{u} = d\bar{u}/dz|_w z$ and $\bar{u} = U$ (figure 4a, c), i.e. $\delta_u = U/(d\bar{u}/dz|_w)$, while the thermal boundary-layer thickness, δ_T is defined as the wall-normal distance to the intercept of $\bar{T} = T_h + d\bar{T}/dz|_w z$ and $\bar{T} = T_h - \Delta T/2$ (figure 4b, d), i.e. $\delta_T = -(\Delta T/2)/(d\bar{T}/dz|_w)$. These boundary-layer definitions conveniently distinguish the boundary-layer behaviour of the flow from the bulk behaviour and this is demonstrated for two representative Ra in figure 4. In figure 4(a, c), the kinetic dissipation due to the mean, $\bar{\varepsilon}_{\bar{u}} \equiv \nu(\partial\bar{u}_i/\partial x_j)^2 = \nu(d\bar{u}/dz)^2$, overwhelms the kinetic dissipation due to the turbulent fluctuations, $\bar{\varepsilon}_{u'} \equiv \nu(\partial u'_i/\partial x_j)^2$ in the kinetic boundary layer. Similarly, in figure 4(b, d), the thermal dissipation due to the mean, $\bar{\varepsilon}_{\bar{T}} \equiv \kappa(\partial\bar{T}/\partial x_j)^2 = \kappa(d\bar{T}/dz)^2$, overwhelms the thermal dissipation due to the turbulent fluctuations, $\bar{\varepsilon}_{T'} \equiv \kappa(\partial T'/\partial x_j)^2$, in the thermal boundary layer. Both profiles of $\bar{\varepsilon}_{u'}$ and $\bar{\varepsilon}_{T'}$ exhibit characteristics similar to that found in RB convection: the profiles peak at the wall and are approximately flat in the bulk (e.g. Emran & Schumacher 2008; Kaczorowski & Wagner 2009; Kaczorowski & Xia 2013). Alternative boundary-layer definitions such as the crossover locations between the mean dissipations and fluctuation dissipations, δ_u^d and δ_T^d , as well as the displacement thickness, $\delta^* \equiv \int_0^{\delta_{max}} (1 - \bar{u}/\bar{u}_{max}) dz$, where $\bar{u}(\delta_{max}) = \bar{u}_{max}$, are found to provide similar scaling characteristics, as verified in figure 5.

For comparison, we compute the Prandtl–Blasius–Pohlhausen boundary-layer thicknesses for vertical natural convection from the laminar similarity scaling, which is different to its horizontal counterpart. Using the definitions for δ_u , δ_T (figure 4) and wind-based Re from (3.1 c) and for $Pr = 0.709$, we obtain, by setting $x/H = 1$ in the laminar similarity scaling (see White 1991, § 4-13.3):

$$\delta_u/H \approx 0.43 Re^{-1/2}, \quad \delta_T/H \approx 2.10 Re^{-1/2}. \quad (3.2a,b)$$

Varying x/H , pertaining to the wall-parallel coherence of the wind, would merely al-

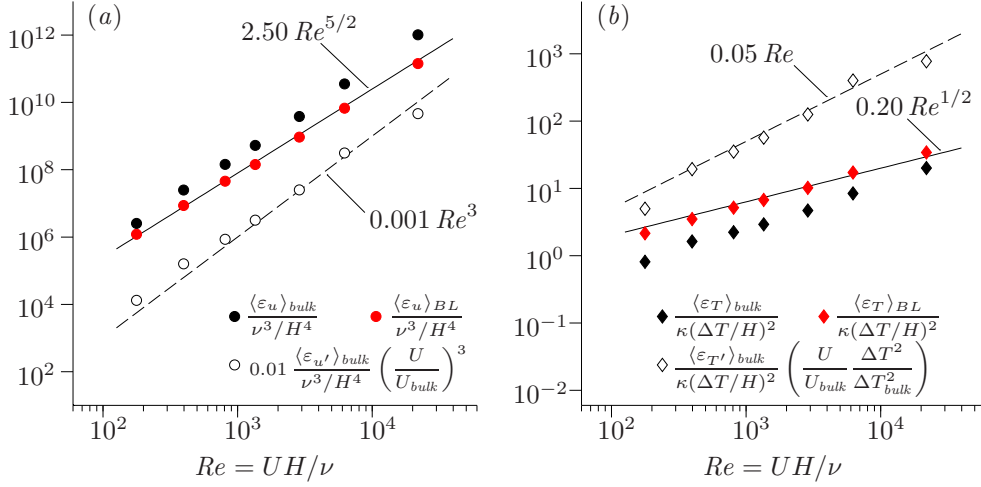


Figure 6: Dissipation trends in the boundary layer and bulk for (a) $\langle \varepsilon_u \rangle$ and (b) $\langle \varepsilon_T \rangle$. The figures show that $\langle \varepsilon_u \rangle_{BL} \sim Re^{5/2}$, whilst $\langle \varepsilon_T \rangle_{bulk} \sim \langle \varepsilon_T \rangle_{BL} \sim Re^{1/2}$. Also shown are bulk dissipations of turbulent fluctuations which vary as $\langle \varepsilon_{u'} \rangle_{bulk} \sim Re^3$ (o) and $\langle \varepsilon_{T'} \rangle_{bulk} \sim Re$ (◊).

ter the coefficients in (3.2). In figure 5, the boundary-layer thicknesses using the slope definition from figure 4, i.e. δ_u and δ_T , the dissipation crossover definitions, δ_u^d and δ_T^d , and displacement thickness δ^* , are compared with (3.2a, b). Using a least-squares fit of the present data to a power law, we find that $\delta_u/H \sim Re^{-0.45}$ and $\delta_T/H \sim Re^{-0.60}$ (not shown in figure 5) which is in fair agreement to the $Re^{-1/2}$ trend, in accordance to the laminar predictions from the GL theory. Hence, for simplicity, we will adopt the boundary-layer definitions based on δ_u and δ_T hereafter. An upper bound for the boundary layers can be obtained when both boundary-layer and bulk regions are laminar. In this case, the velocity profile is a cubic and the temperature profile is linear, from which $\delta_u/H \approx 0.096$ and $\delta_T/H = 0.5$. For reference, the laminar-to-turbulent transition which occurs at $(Re_{\delta^*})_{cr} \equiv (U\delta^*/\nu)_{cr} \approx 420$, where δ^* is the displacement thickness (Landau & Lifshitz 1987), is also shown in figure 5, to the right of all present data. Consistent with the insight provided by the GL theory, the boundary layers in vertical natural convection for the present Ra range cannot be considered as turbulent boundary layers. Instead, they can be interpreted as laminar boundary layers animated by the turbulent wind.

Figure 5 shows that $\delta_T > \delta_u$ in all cases considered here at $Pr = 0.709$. This situation is expected to be reversed ($\delta_u > \delta_T$) when $Pr > 1$ (Grossmann & Lohse 2001). At transitional Ra and at high Pr , an oscillatory flow regime is found in vertical natural convection (Chait & Korpela 1989) and it remains unknown whether this oscillatory flow persists at higher Ra and whether (3.1 b) accounts for this behaviour.

3.2. Boundary-layer and bulk contributions to the dissipations

The GL theory splits the global-averaged kinetic and thermal dissipation rates into contributions from the boundary layer and bulk regions (figure 1) such that

$$\langle \varepsilon_u \rangle = \langle \varepsilon_u \rangle_{BL} + \langle \varepsilon_u \rangle_{bulk} = \frac{2}{H} \int_0^{\delta_u} \nu \left(\frac{\partial u_i}{\partial x_j} \right)^2 dz + \frac{2}{H} \int_{\delta_u}^{H/2} \nu \left(\frac{\partial u_i}{\partial x_j} \right)^2 dz, \quad (3.3a)$$

$$\langle \varepsilon_T \rangle = \langle \varepsilon_T \rangle_{BL} + \langle \varepsilon_T \rangle_{bulk} = \frac{2}{H} \int_0^{\delta_T} \kappa \left(\frac{\partial T}{\partial x_j} \right)^2 dz + \frac{2}{H} \int_{\delta_T}^{H/2} \kappa \left(\frac{\partial T}{\partial x_j} \right)^2 dz, \quad (3.3b)$$

cf. (2.9) and (2.10) in Grossmann & Lohse (2000), where the time- and volume-average is denoted by $\langle \cdot \rangle$. Following the GL theory, once the wind that acts on the boundary layer is identified as U , the kinetic boundary-layer dissipation, $\langle \varepsilon_u \rangle_{BL}$, is approximated using the wall-normal gradient of the streamwise velocity, i.e. $\nu(\partial u_i/\partial x_j)^2 \approx \nu(U/\delta_u)^2$, over the volume fraction, δ_u/H . Similarly, the thermal boundary-layer dissipation, $\langle \varepsilon_T \rangle_{BL}$, is approximated using the wall-normal gradient of the temperature, i.e. $\kappa(\partial T/\partial x_j)^2 \approx \kappa(\Delta T/\delta_T)^2$, over the volume-fraction δ_T/H . The boundary-layer terms on the right-hand side of (3.3a, b) can thus be written as,

$$\langle \varepsilon_u \rangle_{BL} \sim \nu \frac{U^2}{\delta_u^2} \left(\frac{\delta_u}{H} \right) \sim \nu \frac{U^2}{\delta_u^2} \left(Re^{-1/2} \right) = \frac{\nu^3}{H^4} Re^{5/2}, \quad (3.4a)$$

$$\langle \varepsilon_T \rangle_{BL} \sim \kappa \frac{\Delta T^2}{\delta_T^2} \left(\frac{\delta_T}{H} \right) \sim \kappa \frac{\Delta T^2}{\delta_T^2} \left(Re^{-1/2} f(Pr) \right) = \kappa \frac{\Delta T^2}{H^2} Re^{1/2} f(Pr), \quad (3.4b)$$

where the expressions for δ_u/H and δ_T/H in (3.1a, b) are used. On the other hand, the bulk dissipation terms are modelled as

$$\langle \varepsilon_u \rangle_{bulk} \sim \frac{U^3}{H} = \frac{\nu^3}{H^4} Re^3, \quad \langle \varepsilon_T \rangle_{bulk} \sim \frac{U \Delta T^2}{H} = \kappa \frac{\Delta T^2}{H^2} Pr Re, \quad (3.5a, b)$$

which follow from dimensional arguments of the turbulence cascade in the bulk region. In this region, larger eddies transfer energy to smaller eddies. Thus, the dissipation rate can be thought to scale with the largest eddies with energy of order U^2 and timescale H/U , independent of ν . Similarly, the thermal dissipation rate can be thought to scale with the largest eddies with variance of order ΔT^2 and timescale H/U , independent of κ (see Pope 2000). Figure 6(a, b) show the trends of the boundary-layer and bulk contributions. In figure 6(a), although $\langle \varepsilon_u \rangle_{BL} \sim Re^{5/2}$ and $\langle \varepsilon_u \rangle_{bulk} \sim Re^3$ as predicted in (3.4a) and (3.5a), the ratio of boundary-layer-to-bulk contributions for thermal dissipation appears constant as shown by the parallel trends of $\langle \varepsilon_T \rangle_{BL}$ and $\langle \varepsilon_T \rangle_{bulk}$ in figure 6(b). This seemingly contradicts the $\langle \varepsilon_T \rangle_{BL} \sim Re^{1/2}$ and $\langle \varepsilon_T \rangle_{bulk} \sim Re$ predictions for the boundary-layer and bulk thermal dissipations, (3.4b) and (3.5b). A similar behaviour is reported by Grossmann & Lohse (2004) based on a DNS study of RB convection by Verzicco & Camussi (2003). The reason is that plumes, which provide the scaling in (3.4b), are also present in the bulk, as discussed in Grossmann & Lohse (2004).

It seems unexpected that the classical cascade arguments that lead to the Re scaling for $\varepsilon_{T,bulk}$ are not observed in the present flow. Presently, we consider the possibility that the turbulent scalings in the bulk are obscured by a strong mean component. To observe this behaviour, we subtract the bulk dissipation of the mean,

$$\langle \varepsilon_{u'} \rangle_{bulk} = \langle \varepsilon_u \rangle_{bulk} - \langle \varepsilon_{\bar{u}} \rangle_{bulk}, \quad \langle \varepsilon_{T'} \rangle_{bulk} = \langle \varepsilon_T \rangle_{bulk} - \langle \varepsilon_{\bar{T}} \rangle_{bulk}, \quad (3.6a, b)$$

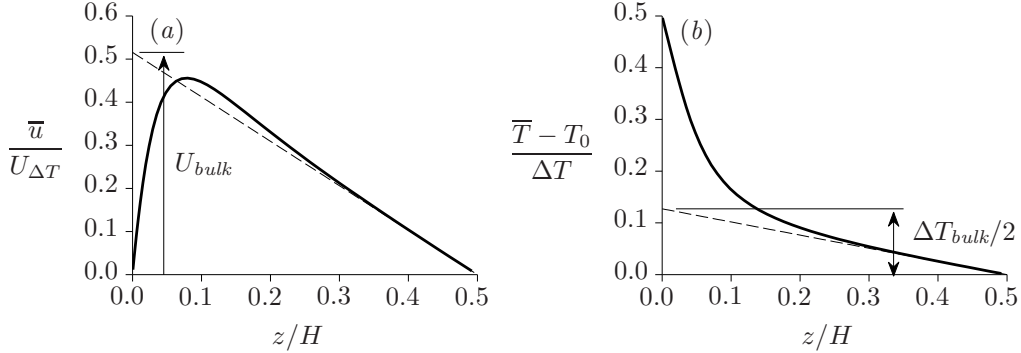


Figure 7: Illustrations of (a) U_{bulk} and (b) ΔT_{bulk} for $Ra = 5.4 \times 10^5$. Specifically, they are defined as $U_{bulk} = -(H/2) d\bar{u}/dz|_c$ and $\Delta T_{bulk} = -H d\bar{T}/dz|_c$, where $(\cdot)|_c$ denotes the centreline value, refer to (3.8).

where,

$$\langle \varepsilon_{\bar{u}} \rangle_{bulk} = \frac{2}{H} \int_{\delta_u}^{H/2} \nu \left(\frac{d\bar{u}}{dz} \right)^2 dz, \quad \langle \varepsilon_{\bar{T}} \rangle_{bulk} = \frac{2}{H} \int_{\delta_T}^{H/2} \kappa \left(\frac{d\bar{T}}{dz} \right)^2 dz. \quad (3.7a,b)$$

For RB convection, the global average of (3.7 a) is zero although (3.7 b) is non-zero. Indeed, it will be shown that the strong mean components in vertical natural convection, ΔT_{bulk} and U_{bulk} , drive the turbulent fluctuations, as discussed in Grossmann & Lohse (2004) in the context of RB convection. Here, we define ΔT_{bulk} and U_{bulk} using their corresponding centreline mean gradients (figure 7),

$$\Delta T_{bulk} = -H \left. \frac{d\bar{T}}{dz} \right|_c, \quad U_{bulk} = -\frac{H}{2} \left. \frac{d\bar{u}}{dz} \right|_c, \quad (3.8a,b)$$

where $(\cdot)|_c$ denotes the centreline value. Thus, the bulk dissipations due to fluctuating quantities may now scale as

$$\langle \varepsilon_{u'} \rangle_{bulk} \sim \frac{U_{bulk}^3}{H} = \frac{\nu^3}{H^4} Re^3 \left(\frac{U_{bulk}}{U} \right)^3, \quad (3.9a)$$

$$\langle \varepsilon_{T'} \rangle_{bulk} \sim \frac{U_{bulk} \Delta T_{bulk}^2}{H} = \kappa \frac{\Delta T^2}{H^2} Pr Re \left(\frac{U_{bulk}}{U} \frac{\Delta T_{bulk}}{\Delta T} \right), \quad (3.9b)$$

where the wind-based Reynolds number scaling, Re , is defined as before. In figure 6(a, b), we find that the trends predicted by (3.9) for $\langle \varepsilon_{u'} \rangle_{bulk}$ and $\langle \varepsilon_{T'} \rangle_{bulk}$ agree with the power-laws of the GL theory for bulk dissipation (3.5), and are consistent with the Kolmogorov–Obukhov–Corrsin scaling in the bulk region. Thus, to fully extend the GL theory to the present flow, (3.7) and (3.9) need to be closed with models for U_{bulk}/U , $\Delta T_{bulk}/\Delta T$ and the bulk dissipation of the mean, i.e. $\langle \varepsilon_{\bar{u}} \rangle_{bulk}$ and $\langle \varepsilon_{\bar{T}} \rangle_{bulk}$, in terms of Re , Ra , Nu and Pr .

3.3. Global averages for kinetic and thermal dissipations

For both RB and vertical natural convection, the global-averaged dissipation rates in (3.3) take the exact forms,

$$\langle \varepsilon_u \rangle = \frac{\nu^3}{H^4} \frac{\langle -u_g T \rangle}{\kappa \Delta T / H} \frac{Ra}{Pr^2}, \quad \langle \varepsilon_T \rangle = \kappa \frac{\Delta T^2}{H^2} Nu, \quad (3.10a,b)$$

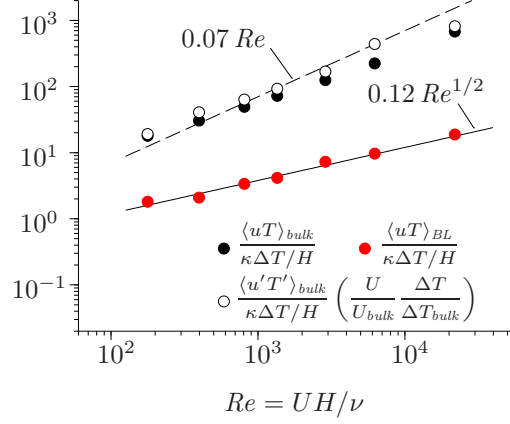


Figure 8: Trends of the buoyancy flux, $\langle uT \rangle$, showing $\langle uT \rangle_{BL} \sim Re^{1/2}$ and $\langle u'T' \rangle_{bulk} \sim Re$. The boundary-layer and bulk components are decomposed using $\delta_u = U/(\mathrm{d}\bar{u}/\mathrm{d}z|_w)$, as before.

where u_g is velocity component in the direction of gravity. In RB convection, $\langle -u_g T \rangle = \langle wT \rangle = f_w - \langle \kappa \mathrm{d}\bar{T}/\mathrm{d}z \rangle$, and it can thus be shown that $\langle \epsilon_u \rangle_{RB} = (\nu^3/H^4)(Nu - 1)(Ra/Pr^2)$, cf. (9) and (10) in Ahlers *et al.* (2009). In contrast, $\langle -u_g T \rangle = \langle uT \rangle$ for vertical natural convection and the relations remain unclosed. However, if we apply the same GL-theory scaling arguments for boundary-layer contribution i.e. $\langle uT \rangle_{BL}$, and the same GL-theory scaling arguments for the turbulent bulk contribution, i.e. $\langle u'T' \rangle_{bulk} = \langle uT \rangle_{bulk} - \langle \bar{u}\bar{T} \rangle_{bulk}$, as before, we obtain,

$$\langle uT \rangle_{BL} \sim U \Delta T \frac{\delta_u}{H} = \kappa \frac{\Delta T}{H} Pr Re \left(\frac{\delta_u}{H} \right) \sim \kappa \frac{\Delta T}{H} Pr Re^{1/2}, \quad (3.11a)$$

$$\langle u'T' \rangle_{bulk} \sim U_{bulk} \Delta T_{bulk} = \kappa \frac{\Delta T}{H} Pr Re \left(\frac{U_{bulk} \Delta T_{bulk}}{U \Delta T} \right). \quad (3.11b)$$

In figure 8, we find that $\langle uT \rangle_{BL} \sim Re^{1/2}$ and $\langle u'T' \rangle_{bulk} \sim Re$, in agreement with (3.11) and corroborating the GL theory of differing physics in the boundary layer and bulk regions. Similar to the thermal dissipation discussed in §3.2, the contamination of the bulk region by plumes released from the laminar boundary layer (Grossmann & Lohse 2004) results in a scaling exponent for the bulk contribution that is less than 1 but larger than 1/2 (compare figures 6 b and 8). This suggests a possible approach for modelling the unclosed buoyancy flux (3.10 a) once appropriate models can be found for U_{bulk}/U , $\Delta T_{bulk}/\Delta T$ and the mean component of the buoyancy flux, i.e. $\langle \bar{u}\bar{T} \rangle_{bulk}$.

4. Conclusions

The present DNS data for vertical natural convection with Ra ranging between 1.0×10^5 and 1.0×10^9 and $Pr = 0.709$ demonstrate the general applicability of the GL theory which was originally developed for RB convection. In agreement with the theory, the $Nu \sim Ra^p$ relationship for vertical natural convection exhibits neither a 1/3- nor a 1/4-power scaling due to the different physics of the boundary layer (or plume) and bulk (or background). Thus, the dissipation in the boundary layer and bulk, (3.3), are expected to scale differently as proposed by the GL theory. Similar to RB convection, the boundary-layer thicknesses of velocity and temperature for vertical natural convection

exhibit laminar-like scaling, i.e. $\delta_u/H \sim Re^{-1/2}$ and $\delta_T/H \sim Re^{-1/2}$ (figure 5), where the wind-based Reynolds number is defined as $Re \equiv UH/\nu$. For the present configuration, the “wind” is readily identified from the non-zero plane-averaged streamwise velocity, $U = \bar{u}_{max}$. In the boundary layers, the kinetic and thermal dissipations scale as predicted by the GL theory, (3.4), i.e. $\langle \varepsilon_u \rangle_{BL} \sim Re^{5/2}$ and $\langle \varepsilon_T \rangle_{BL} \sim Re^{1/2}$ (figure 6). In the bulk region, the Kolmogorov–Obukhov–Corrsin scaling, i.e. $\langle \varepsilon_{u'} \rangle_{bulk} \sim Re^3$ and $\langle \varepsilon_{T'} \rangle_{bulk} \sim Re$, are recovered once the dissipations of the mean are subtracted from the bulk dissipations (figure 6). These are consistent with the power laws originally predicted by the GL theory, (3.5). Unlike RB convection, the global kinetic dissipation (3.10 *a*) cannot be determined *a priori* because a relationship between the buoyancy flux is unclosed. One possible closure for this relationship is by using the laminar-like boundary-layer scaling and the turbulent bulk scaling as prescribed by the GL theory (§3.3). When applied, the buoyancy flux is found to scale as $\langle uT \rangle_{BL} \sim Re^{1/2}$ and $\langle u'T' \rangle_{bulk} \sim Re$ (figure 8), consistent with the GL prediction. Hence, to fully extend the GL theory to the present flow, relationships for the bulk dissipation of the mean, $\langle \varepsilon_{\bar{u}} \rangle_{bulk}$ and $\langle \varepsilon_{\bar{T}} \rangle_{bulk}$; mean components influencing the bulk, U_{bulk}/U and $\Delta T_{bulk}/\Delta T$; and mean vertical buoyancy flux, $\langle \bar{u}\bar{T} \rangle_{bulk}$, are needed in terms of Re , Ra , Nu and Pr . Current efforts are underway to uncover the aforementioned relationships. Similar to RB convection, the present results indicate that, for vertical natural convection, Ra , Nu and Pr may be better related by non-pure power laws that reflect the underlying flow physics.

Acknowledgements

The authors gratefully acknowledge the computing time provided by the NCI National Facility in Canberra, Australia, which is supported by the Australian Commonwealth Government. Some of the simulations were conducted with the support of iVEC through the use of advanced computing resources located at iVEC@Murdoch, Western Australia, Australia.

REFERENCES

- AHLERS, G., GROSSMANN, S. & LOHSE, D. 2009 Heat transfer and large scale dynamics in turbulent Rayleigh–Bénard convection. *Rev. Mod. Phys.* **81**, 503–537.
- BATCHELOR, G. K. 1954 Heat transfer by free convection across a closed cavity between vertical boundaries at different temperatures. *Q. Appl. Math.* **12**, 209–233.
- CALZAVARINI, E., DOERING, C. R., GIBBON, J. D., LOHSE, D., TANABE, A. & TOSCHI, F. 2006 Exponentially growing solutions in homogeneous Rayleigh–Bénard convection. *Phys. Rev. E* **73** (3), 035301.
- CALZAVARINI, E., LOHSE, D., TOSCHI, F. & TRIPICCIONE, R. 2005 Rayleigh and Prandtl number scaling in the bulk of Rayleigh–Bénard turbulence. *Phys. Fluids* **17**, 055107.
- CASTAING, B., GUNARATNE, G., HESLOT, F., KADANOFF, L., LIBCHABER, A., THOMAE, S., WU, X.-Z., ZALESKI, S. & ZANETTI, G. 1989 Scaling of hard thermal turbulence in Rayleigh–Bénard convection. *J. Fluid Mech.* **204**, 1–30.
- CHAIT, A. & KORPELA, S. A. 1989 The secondary flow and its stability for natural convection in a tall vertical enclosure. *J. Fluid Mech.* **200**, 189–216.
- CHAVANNE, X., CHILLÀ, F., CASTAING, B., HÉBRAL, B., CHABAUD, B. & CHAUSSY, J. 1997 Observation of the ultimate regime in Rayleigh–Bénard convection. *Phys. Rev. Lett.* **79** (19), 3648–3651.
- CHAVANNE, X., CHILLÀ, F., CHABAUD, B., CASTAING, B. & HÉBRAL, B. 2001 Turbulent Rayleigh–Bénard convection in gaseous and liquid He. *Phys. Fluids* **13** (5), 1300–1320.
- CHURCHILL, S. W. & CHU, H. H. S. 1975 Correlating equations for laminar and turbulent free convection from a vertical plate. *Int. J. Heat Mass Transfer* **18**, 1323–1329.

- ECKHARDT, B., GROSSMANN, S. & LOHSE, D. 2007 Torque scaling in turbulent Taylor–Couette flow between independently rotating cylinders. *J. Fluid Mech.* **581**, 221–250.
- ELDER, J. W. 1965 Turbulent free convection in a vertical slot. *J. Fluid Mech.* **23**, 99–111.
- EMRAN, M. S. & SCHUMACHER, J. 2008 Fine-scale statistics of temperature and its derivatives in convective turbulence. *J. Fluid Mech.* **611**, 13–34.
- GEORGE, W. K. & CAPP, S. P. 1979 A theory for natural convection turbulent boundary layers next to heated vertical surfaces. *Int. J. Heat Mass Transfer* **22**, 813–826.
- GROSSMANN, S. & LOHSE, D. 2000 Scaling in thermal convection: a unifying theory. *J. Fluid Mech.* **407**, 27–56.
- GROSSMANN, S. & LOHSE, D. 2001 Thermal convection at large Prandtl numbers. *Phys. Rev. Lett.* **86**, 3316–3319.
- GROSSMANN, S. & LOHSE, D. 2002 Prandtl and Rayleigh number dependence of the Reynolds number in turbulent thermal convection. *Phys. Rev. E* **66** (1), 016305.
- GROSSMANN, S. & LOHSE, D. 2004 Fluctuations in turbulent Rayleigh–Bénard convection: the role of plumes. *Phys. Fluids* **16**, 4462–4472.
- KACZOROWSKI, M. & WAGNER, C. 2009 Analysis of the thermal plumes in turbulent Rayleigh–Bénard convection based on well-resolved numerical simulations. *J. Fluid Mech.* **618**, 89–112.
- KACZOROWSKI, M. & XIA, K.-Q. 2013 Turbulent flow in the bulk of Rayleigh–Bénard convection: small-scale properties in a cubic cell. *J. Fluid Mech.* **722**, 596–617.
- KIŠ, P. & HERWIG, H. 2012 The near wall physics and wall functions for turbulent natural convection. *Int. J. Heat Mass Transfer* **55**, 2625–2635.
- LANDAU, L. D. & LIFSHITZ, E. M. 1987 *Fluid Mechanics*, 2nd edn. Pergamon Press.
- NG, C. S. 2013 Direct numerical simulation of natural convection bounded by differentially heated vertical walls. Master’s thesis, University of Melbourne.
- NG, C. S., CHUNG, D. & OOI, A. 2013 Turbulent natural convection scaling in a vertical channel. *Int. J. Heat Fluid Flow* **44**, 554–562.
- PALLARES, J., VERNET, A., FERRE, J. A. & GRAU, F. X. 2010 Turbulent large-scale structures in natural convection vertical channel flow. *Int. J. Heat Mass Transfer* **53**, 4168–4175.
- POPE, S. B. 2000 *Turbulent Flows*. Cambridge University Press.
- SCHEEL, J. D. & SCHUMACHER, J. 2014 Local boundary layer scales in turbulent Rayleigh–Bénard convection. *J. Fluid Mech.* **758**, 344–373.
- SCHMIDT, L. E., CALZAVARINI, E., LOHSE, D., TOSCHI, F. & VERZICCO, R. 2012 Axially homogeneous Rayleigh–Bénard convection in a cylindrical cell. *J. Fluid Mech.* **691**, 52–68.
- STEVENS, R. J. A. M., CLERCX, H. J. H. & LOHSE, D. 2010a Boundary layers in rotating weakly turbulent Rayleigh–Bénard convection. *Phys. Fluids* **22**, 085103.
- STEVENS, R. J. A. M., LOHSE, D. & VERZICCO, R. 2011 Prandtl and Rayleigh number dependence of heat transport in high Rayleigh number thermal convection. *J. Fluid Mech.* **688**, 31–43.
- STEVENS, R. J. A. M., VAN DER POEL, E. P., GROSSMANN, S. & LOHSE, D. 2013 The unifying theory of scaling in thermal convection: the updated prefactors. *J. Fluid Mech.* **730**, 295–308.
- STEVENS, R. J. A. M., VERZICCO, R. & LOHSE, D. 2010b Radial boundary layer structure and Nusselt number in Rayleigh–Bénard convection. *J. Fluid Mech.* **643**, 495–507.
- SUN, C., CHEUNG, Y.-H. & XIA, K.-Q. 2008 Experimental studies of the viscous boundary layer properties in turbulent Rayleigh–Bénard convection. *J. Fluid Mech.* **605**, 79–113.
- TSUJI, T. & NAGANO, Y. 1988 Characteristics of a turbulent natural convection boundary layer along a vertical flat plate. *Int. J. Heat Mass Transfer* **31**, 1723–1734.
- VERSTEEGH, T. A. M. & NIEUWSTADT, F. T. M. 1999 A direct numerical simulation of natural convection between two infinite vertical differentially heated walls scaling laws and wall functions. *Int. J. Heat Mass Transfer* **42**, 3673–3693.
- VERZICCO, R. & CAMUSSI, R. 2003 Numerical experiments on strongly turbulent thermal convection in a slender cylindrical cell. *J. Fluid Mech.* **477**, 19–49.
- WHITE, F. M. 1991 *Viscous Fluid Flow*, 2nd edn. McGraw-Hill, Inc.
- ZHOU, Q., STEVENS, R. J. A. M., SUGIYAMA, K., GROSSMANN, S., LOHSE, D. & XIA, K.-Q. 2010 Prandtl–Blasius temperature and velocity boundary-layer profiles in turbulent Rayleigh–Bénard convection. *J. Fluid Mech.* **664**, 297–312.

- ZHOU, Q. & XIA, K.-Q. 2010 Measured instantaneous viscous boundary layer in turbulent Rayleigh–Bénard convection. *Phys. Rev. Lett.* **104**, 104301.